Supplement of Atmos. Chem. Phys., 18, 2139–2154, 2018
https://doi.org/10.5194/acp-18-2139-2018-supplement


Atmospheric Chemistry and Physics
Open Access
EGU

*Supplement of*

# Downwind evolution of the volatility and mixing state of near-road aerosols near a US interstate highway

**Provat K. Saha et al.**

*Correspondence to:* Andrew P. Grieshop (apgriesh@ncsu.edu)

**S1: Supplementary figures**

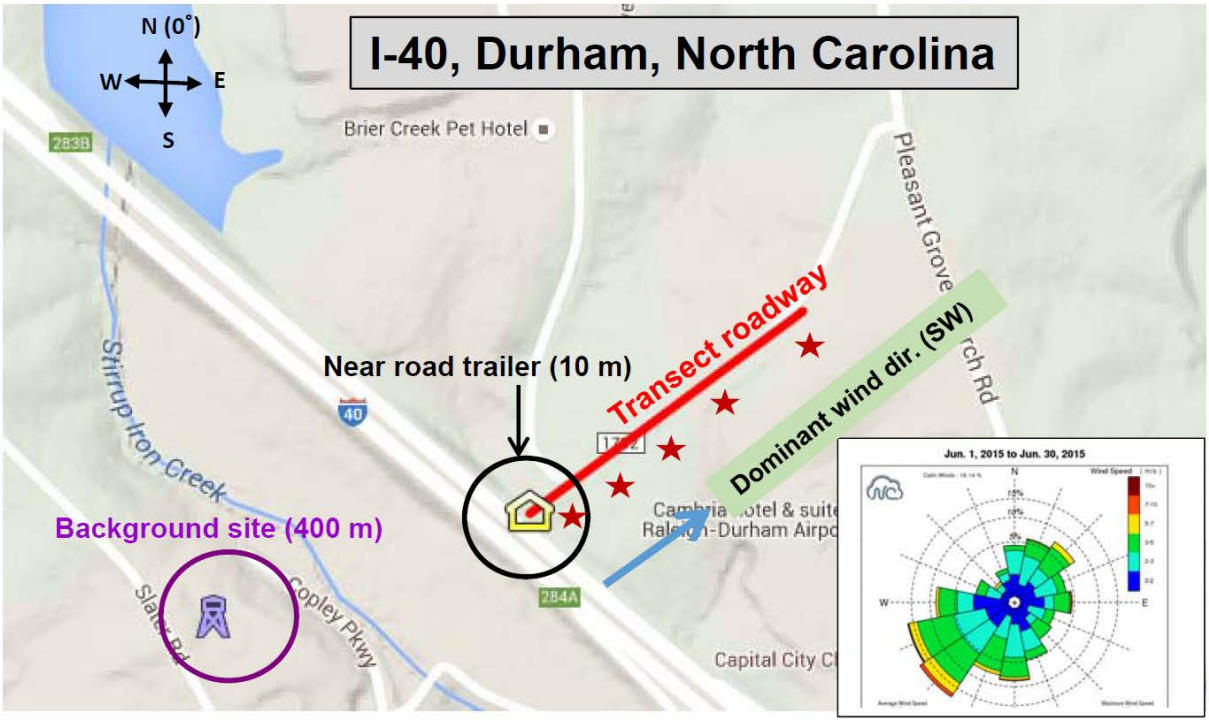


**Figure S1:** Study area map showing near-road trailer, transect roadway and upwind background site. Wind rose plot (inset) is shown for the I-40 summer campaign period (June 1 to June 30, 2015). Image: Google Maps

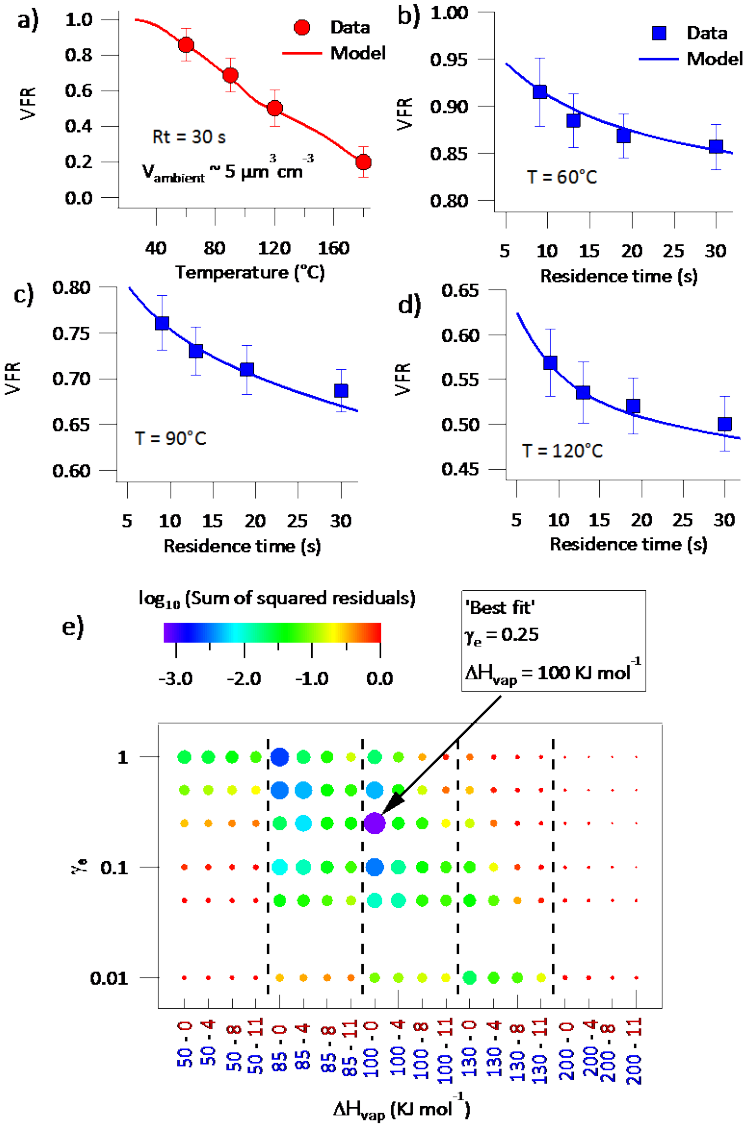


**Figure S2: (**a-d) Measured (point) and modeled (line) campaign-average VFR of $PM_{0.4}$ (integrated volume; 10-400 nm) as a function of TD temperatures and residence times. Measurements were collected in summer 2015 at 10 m distance from the highway. The point is mean, and error bar is ± one standard deviation (~15 minute time resolution data) at each temperature and residence time (Rt) condition. (e) The goodness of fit (sum of squared residuals; SSR) associated with evaporation kinetics model fits to campaign average observations over a wide ranging ($\Delta H_{vap}$ $\gamma_e$) space. A larger marker size indicates a better fit. The x-axis of panel (e) represents $\Delta H_{vap}$ as, $\Delta H_{vap}$ = intercept-slope ($\log_{10}C^*$) (e.g., 50-0 on x-axis indicates intercept = 50 and slope = 0). Fitting approach is described in detail in Saha et al. (2015). Model lines in panels (a-d) are shown using the 'best fit' parameter values ($\Delta H_{vap}$ = 100 kj mol$^{-1}$, $\gamma_e$ = 0.25, and corresponding fitted volatility distribution).

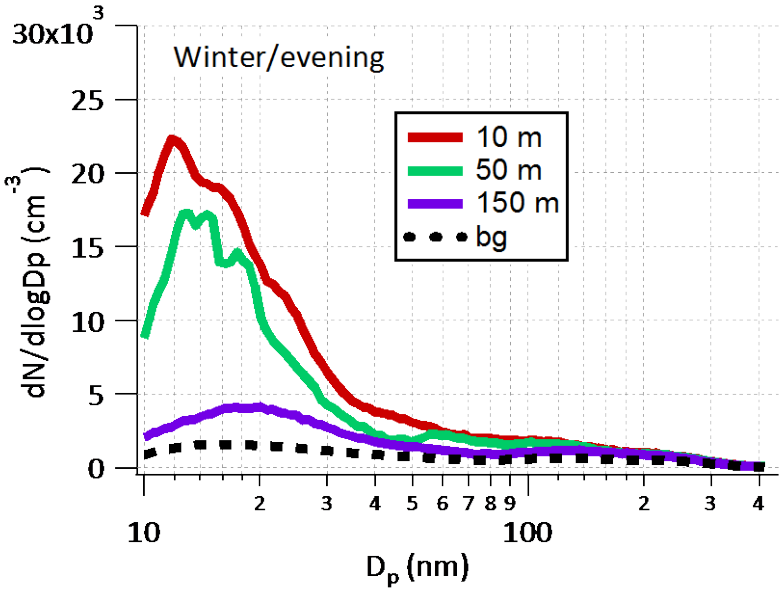


**Figure S3:** Particle number size distributions at different distances from highway. Example data are shown from a transect measurement during I-40 the winter campaign. The background (bg) measurement was collected at approximately 400 m 'upwind' from the main roadside monitor station on the opposite side of I-40.

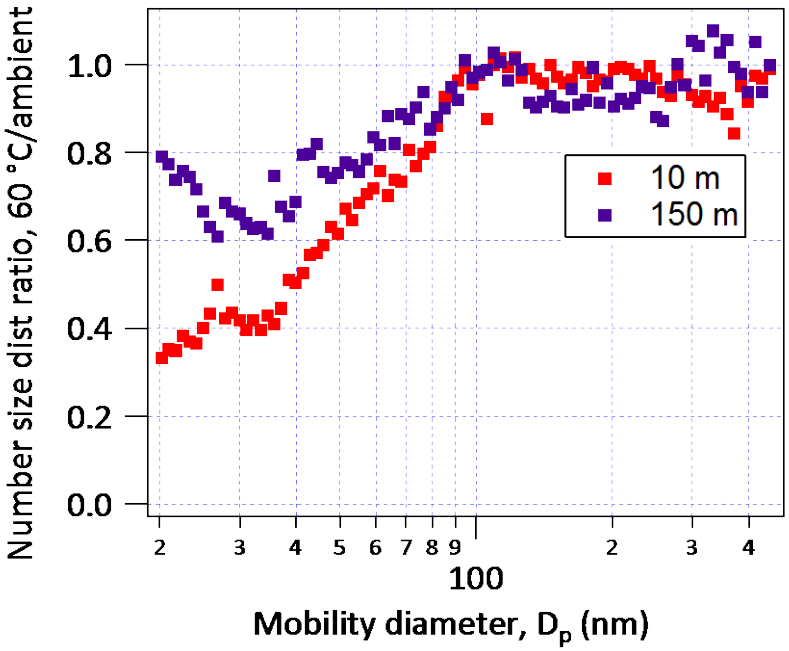


**Figure S4:** Ratio of particle number size distributions (dN/dlogDp) after heating at 60ºC in a thermodenuder (TD) to that at ambient temperature. Example measurements are shown from a typical transect run. Before ratio estimation, particle loss correction factors (as a function of size) were applied to the TD data.

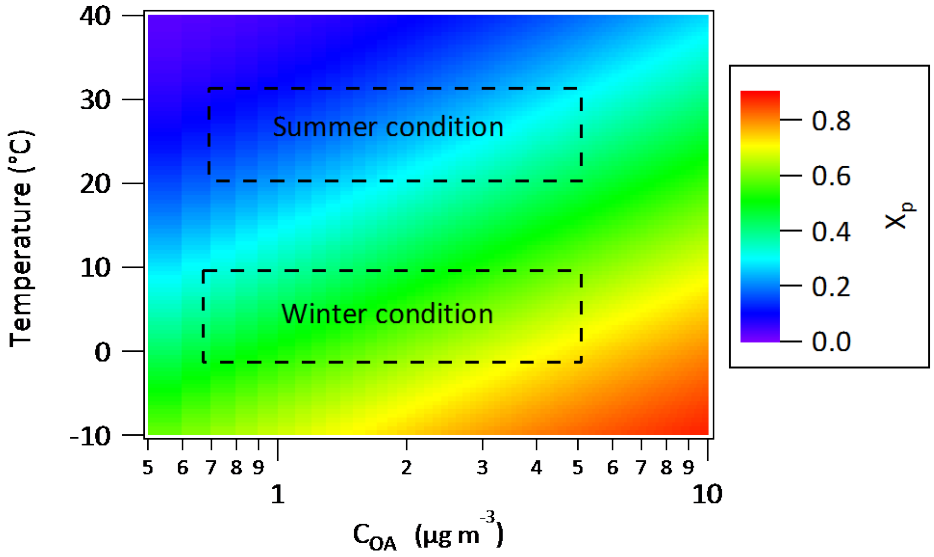


**Figure S5:** Temperature sensitivity of gas-particle partitioning of semi-volatile emissions from motor vehicles. Partitioning calculation uses gasoline POA volatility distribution from May et al. (2013) (TD-GC-MS derived median distribution) and ΔHvap from Ranjan et al. (2012) and method as described in May et al.(2013) and Donahue et al. (2006). $X_p$ refer the fraction of semi-volatile organic mass in the particle-phase.

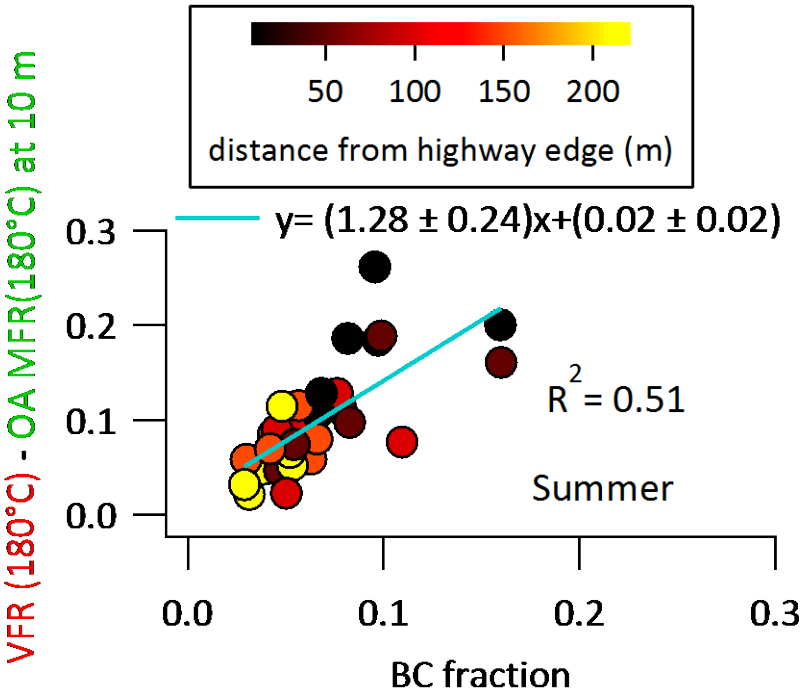


**Figure S6:** Similar to Figure 2(c) in main text, showing analysis for the summer data set. Correlation between the downwind evolution of BC fraction and VFR of $PM_{0.4}$ (at 180 ºC) after subtracting OA MFR (at 180ºC) measured at 10 m using TD/ACSM.

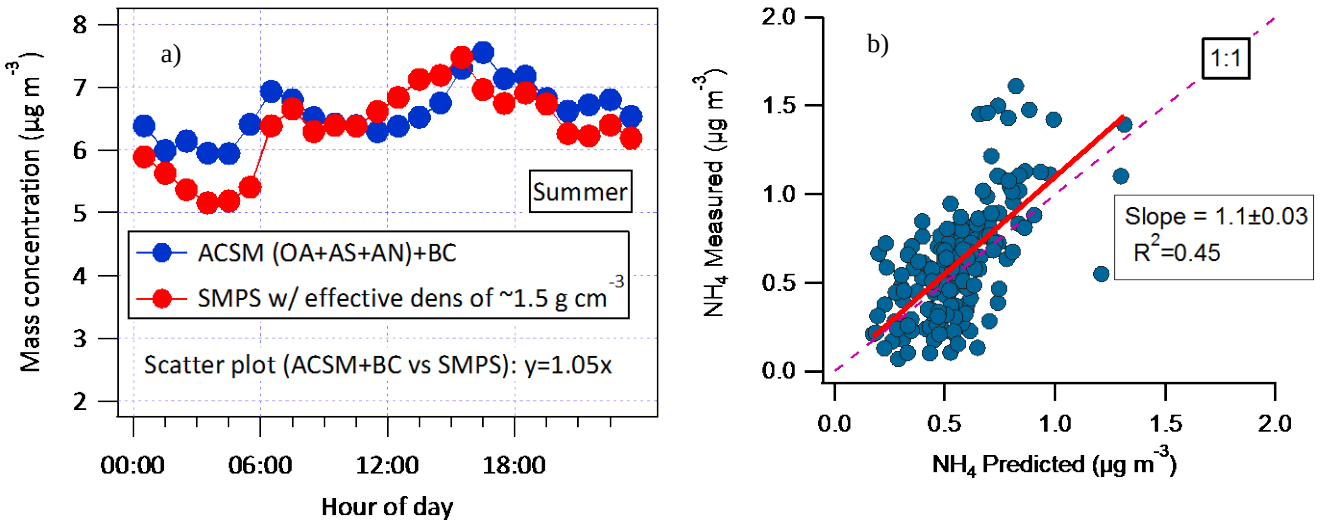


**Figure S7:** a) Comparison of diurnal average submicron ambient aerosol mass concentrations measured by SMPS with the concentrations measured by ACSM [organic aerosol (OA) + ammonium sulfate (AS) + ammonium nitrate (AN)] + PAX [black carbon (BC)]. Campaign-average diurnal profile is shown from summer campaign. ACSM data were analyzed using a collection efficiency (CE) of 1 for all species. AS mass concentration ($m_{as}$) is calculated as $\frac{132}{96} \times m_{SO4}$, where $m_{SO4}$ is the mass concentration of sulfate ($SO_4$). AN mass concentration ($m_{an}$) is calculated as $\frac{80}{62} \times m_{NO3}$, where $m_{NO3}$ is the mass concentration of nitrate ($SO_4$). This calculation assumes that aerosols are neutral. An ammonium balance can provide insights into the validity of assumption of neutral aerosol. Panel (b) shows $NH_4$ measured vs. $NH_4$ predicted plot. The $NH_4$ predicted is estimated as: $NH_4$ predicted = 2*(18/98)*$SO_4$ + (18/63)*$NO_3$ + (18/35)*Cl, where the fractional amounts correspond to the molecular weights of the relevant species. An acidity plot (of measured vs. predicted $NH_4$) has an average slope closer to ~1 (1.1±0.03), indicating an ammonium balance. Therefore, assumption of neutral aerosols at the measurement location was reasonable. SMPS mass concentrations in panel (a) were based on an estimated effective density of submicron aerosols of 1.5 $cm^{-3}$. The effective density is calculated by weighting fractional contribution of different species (e.g., campaign average: OA ~74%, AS ~13%, AN ~7%, and BC ~6%) with their respective densities. Assumed densities for AS, AN, and BC were 1.77, 1.72 and 1.8 g $cm^{-3}$, respectively. An effective density of OA of 1.45 g $cm^{-3}$, estimated from a parameterization by Kuwata et al. (2012) using elemental composition (O:C; H:C). Kuwata et al. (2012) parameterization for OA density was developed based on laboratory data with negligible BC or $NO_3$. Kuwata et al. applied their parameterization to data from the AMAZE campaign, which had an average OA fraction of 0.8 (versus 0.74 for our data), and found that the results agreed well with their measured density. Since our mass comparison based on application of this density to SMPS-measured volume and ACSM+BC mass showed good agreement (Fig. S7a), this indicates our overall estimated effective density, on which OA density has the largest influence, is well constrained.

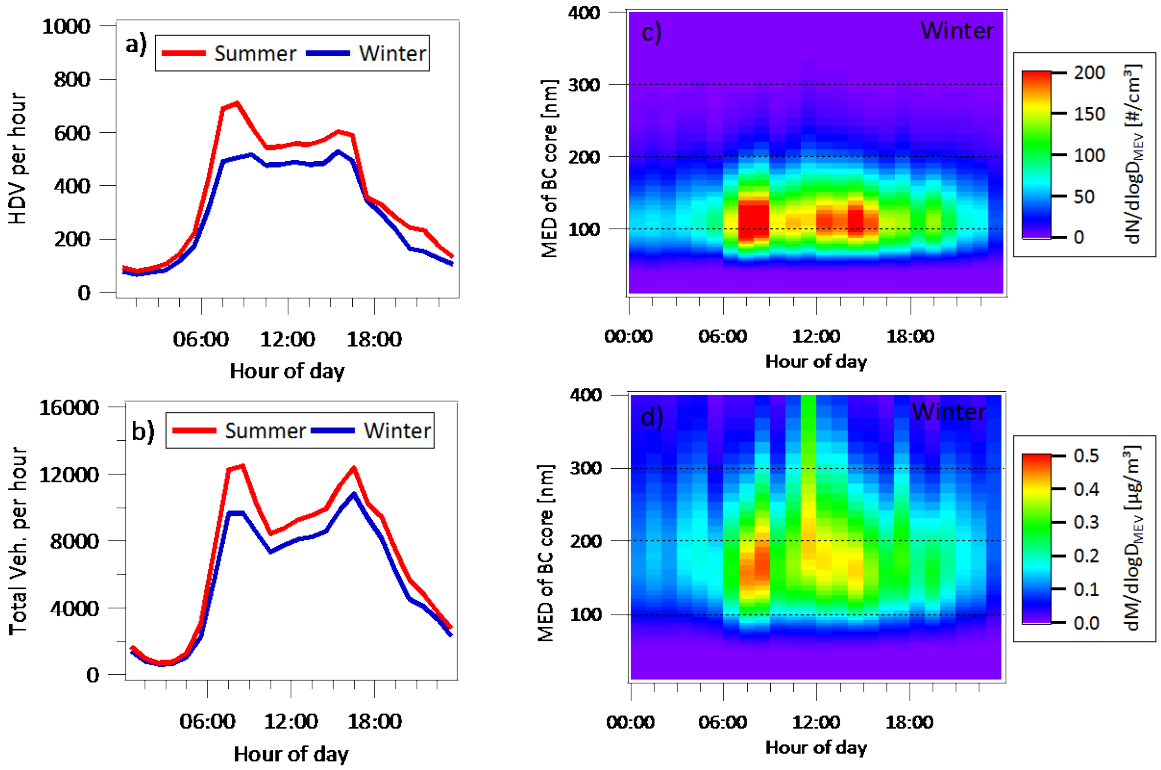


**Figure S8:** (a-b) Campaign-average diurnal profile of traffic volume: a) heavy duty vehicle (HDV), b) total vehicle. (c-d) Campaign-average diurnal profile of SP2-measured BC size distribution: c) number-weighted distribution, d) mass-weighted distribution; MED is the mass equivalent diameter. SP2 data were collected at the roadside trailer (10 m from highway edge) during the I-40 winter campaign only.

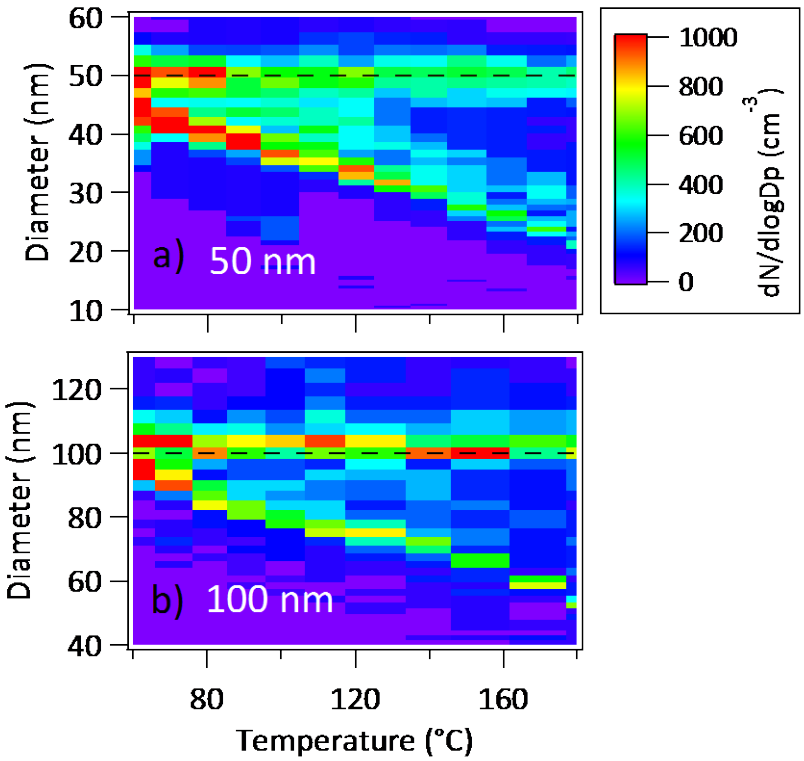


**Figure S9:** Similar to Figure 3 in main text, showing average volatility spectra of 50, and 100 nm particles collected at 10 m distance during the I-40 winter campaign.

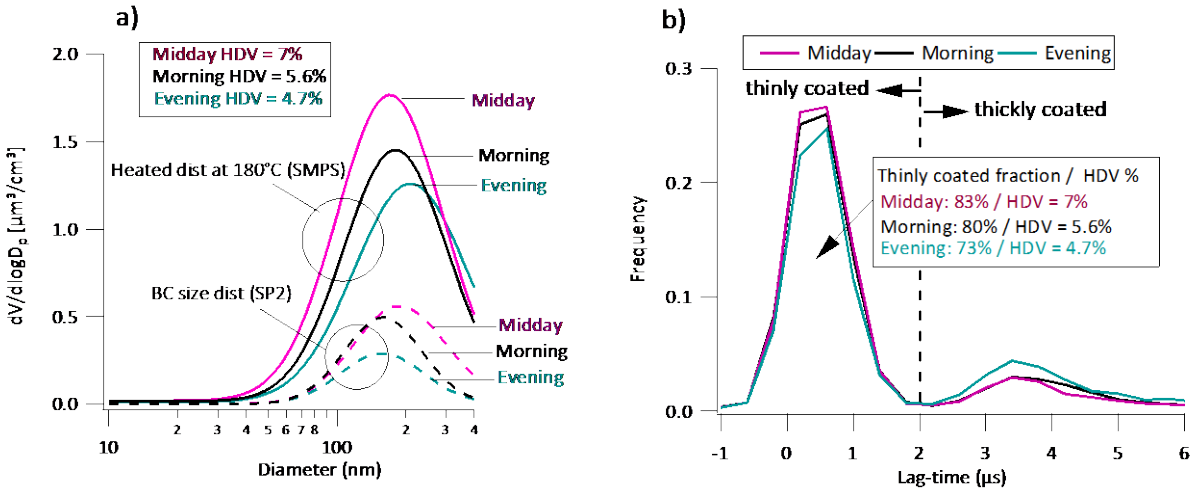


**Figure S10:** (a) Temporal variation of SP2-measured BC size distribution and volume-weighted SMPS size distribution after heating at 180 ºC in a thermodenuder. (b) Temporal variation of the frequency distributions (histograms) of SP2 lag-time ($\Delta\tau$). The analysis shown here is based on an example data set collected at 10 m downwind distance on February 10, 2016 with the wind consistently coming off of the highway.

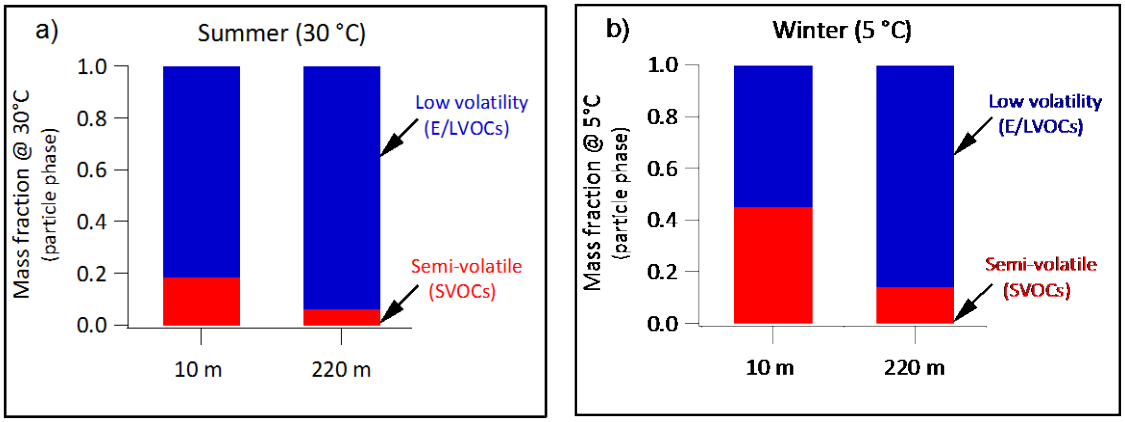


**Figure S11:** Similar to Figure 7 in the main text, showing volatility classification of near-road particles measured at 10 m and 220 m at campaign-average ambient temperature of ~5 ºC in winter and ~30ºC in summer. Distributions of particle-phase material are shown using two broad volatility categories. Partitioning calculation used a $\Delta H_{vap}$ of 100 kj $mol^{-1}$, Clausius–Clapyeron equation and equlibrium partitioning theory (Donahue et al., 2006) for estimating volatility distributions at campaign-average ambient temperatures.

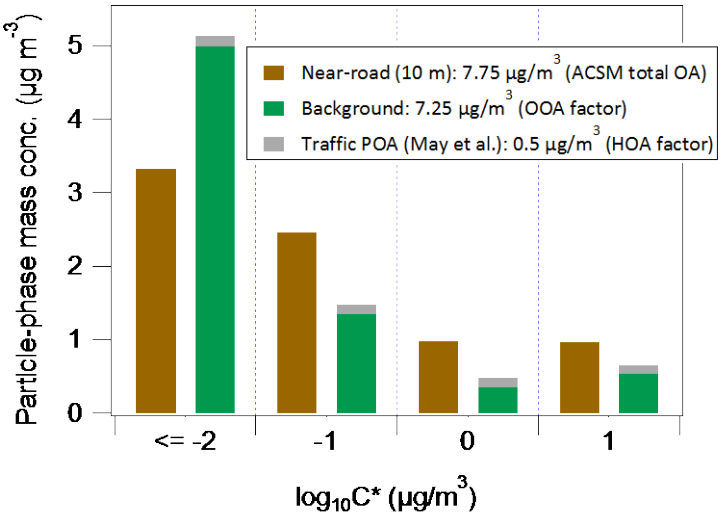


**Figure S12**: Similar to Figure 8b in the main text. In this analysis, traffic and background OA are taken from tracer m/z based factor analysis (Ng et al., 2011) of ACSM-measured mass spectra data at the roadside location. Hydrocarbon-like OA (HOA) is considered as traffic OA and oxygenated-OA (OOA) is considered as background OA. To be consistent with Figure 8, this analysis also considered data from the morning period on June 12, 2015. Figure shows comparison of measured road-side volatility distribution (at 10 m) with the reconstructed distribution using laboratory-measured POA volatility distribution by May et al. (2013) as representative of traffic particles and our measured volatility distribution at far-road location (220 m) as a representative of background particles

**S2: Supplementary tables**

**Table S1:** Assumed TD kinetic model input parameters

| Parameters | Value |
|---|---|
| Diffusion coefficient ($m^2$ $s^{-1}$) | 5 E-06 |
| Surface tension (J $m^{-2}$) | 0.05 |
| Molecular weight (MW) g $mol^{-1}$ | 200 |

**Table S2:** TD-derived volatility distribution (at 25ºC) of near-road aerosols (particle-phase distribution) at 10 m and 220 m downwind distance from the highway I-40 during summer and winter

| logC* at 298K | [a]Particle-phase distribution ($x_i$) | | | |
|---|---|---|---|---|
| | Derived from fitting of observed evaporation of size-selected particles | | | |
| | 10 m (summer) | 220 m (summer) | 10 m (winter) | 220 m (winter) |
| | Combined (25,50,100 nm) | 100 nm | Combined (50,100 nm) | 50 nm |
| -4 | 0.09 | 0.11 | 0.22 | 0.30 |
| -3 | 0.16 | 0.22 | 0.08 | 0.08 |
| -2 | 0.2 | 0.21 | 0.17 | 0.21 |
| -1 | 0.33 | 0.38 | 0.18 | 0.31 |
| 0 | 0.12 | 0.05 | 0.27 | 0.08 |
| 1 | 0.1 | 0.02 | 0.08 | 0.02 |

[a]Reported volatility distributions are fitted with $\gamma_e = 0.25$ and $\Delta H_{vap}$ = 100 KJ $mol^{-1}$ combination

**S3: Conversion equations for TD-fitted particle-phase distribution ($x_i$) to total (gas+particle) distribution ($f_i$) under a gas-particle equilibrium condition.**

$$C_{tot,\mathrm{i}} = \frac{x_i C_{OA}}{\left(1+\frac{C_i^*}{C_{OA}}\right)^{-1}} \qquad \text{[Eq. S1]}$$

$$f_i = \frac{C_{tot,\mathrm{i}}}{\sum C_{tot,\mathrm{i}}} \qquad \text{[Eq. S2]}$$

Here,

$C_{tot,i}$ (μg $m^{-3}$): total vapor- and particle-phase mass concentration of compound *i*,

$C^*_i$ (μg $m^{-3}$): effective saturation concentration of compound *i* at a reference temperature ($T_{ref}$)

$C_{OA}$ (μg $m^{-3}$): total particle-phase organic mass concentration

$x_i$ : mass fraction of compound i found in the particle phase

$f_i$ : fraction of the total vapor and particle-phase contributed by species *i*

Temperature dependent $C_i^*$ is estimated from the Clausius-Clapyeron Equation (Eq. S3)

$$C_i^*(T) = C_i^*(T_{ref}) \exp\left[\frac{\Delta H_{vap,i}}{R}\left(\frac{1}{T_{ref}}-\frac{1}{T}\right)\right]\frac{T_{ref}}{T} \qquad \text{[Eq. S3]}$$

where $\Delta H_{vap}$ (kJ $mol^{-1}$) is the enthalpy of vaporization, $R$ the gas constant, and $T_{ref}$ the reference temperature (298 K).

**S4: Reconstruction of road-side OA volatility distribution combining traffic and background volatility distribution.**

This section describes the analysis approach step-by step those are used for reconstruction of road-side OA volatility distribution combining traffic and background volatility distribution, as shown in Figure 8 and discussed in Sec. 3.4 (main paper)

**a)** Approximate OA mass concentrations at different distance from the highway are estimated from SMPS measurements as: SMPS total mass conc. (function of distance) – BC (function of distance) – inorganics (ACSM at fixed location).

For example, Roadside OA mass at 10 m = SMPS total mass (10 m) - BC (10 m) - inorganics (ACSM at fixed site);

Background OA = SMPS total mass (background) - BC (background) - inorganics (ACSM at fixed site).

An effective density of 1.5 g $cm^{-3}$ (Fig. S7) was used to convert SMPS total volume to total mass.

**b)** Traffic OA at a downwind road-side location is estimated as: total road-side OA - upwind background OA

For example, traffic OA (at 10 m downwind) = total road-side OA (at 10 m downwind) – upwind background OA

**c)** Distribution of road-side OA, traffic OA, and background OA in different volatility bins (i) are calculated as:

$M_{OA}$ (road-side at 10 m)$_i$ = road-side OA mass at 10 m × (TD volatility distribution at 10 m)$_i$

$M_{OA}$ (background)$_i$ = background OA mass × (TD volatility distribution at 220 m)$_i$

$M_{OA}$ (traffic at 10 m)$_i$ = traffic OA mass at 10 m × (Traffic POA volatility distribution from May et. al.)$_i$

**d)** Reconstructed roadside OA volatility distribution is estimated as:

Reconstructed $M_{OA}$ (road-side at 10 m)$_i$ = $M_{OA}$ (traffic at 10 m)$_i$ + $M_{OA}$ (background)$_i$

Finally, we compare this reconstructed distribution with our road-side distribution measured at 10 mm (see Figure 8b of main paper).

**S5: Tracer m/z based factor analysis of ACSM data set**

Tracer m/z based OA components are estimated following Ng et al. (2011) as: hydrocarbon-like OA (HOA ~ 13.4 × ($C_{57}$ − 0.1 × $C_{44}$)) and oxygenated OA (OOA ~ 6.6 × $C_{44}$), where $C_{57}$ and $C_{44}$ are the equivalent mass concentration of tracer ion m/z 57 and 44, respectively. Previous evaluation of this method has shown that it can reproduce the HOA and OOA concentrations to within ~30% of the results from detailed PMF analysis at most sites (Ng. et al. 2011). The estimated traffic-OA (HOA factor) contribution was found to be substantially lower (~5-10x) than that derived based on background-subtracted roadside concentrations measured by SMPS in combination with other data (e..g, Fig. 8a in the main text). Therefore, in analysis shown in Figure S12, the volatility of near-road particles is dominated by contribution from background particles and the combined distribution does a poor job of recreating the observed near-road volatility distribution.

Several factors likely contribute to this discrepancy. For one, since the correlation equations for tracer m/z based factor analysis are empirical (Ng et al., 2011), this method's accuracy and representativeness may be limited in many environments. Further, a substantial fraction of traffic-emitted smaller particles may fall outside of transmission window of ACSM (< 70 nm), but these small particles likely do not have significant contributions to overall mass contribution. On the other hand, measurements of fresh vehicle-emitted particles with an SMPS may be biased high to some extent due to the non-spherical morphology of fresh soot particles (DeCarlo et al., 2004; Maricq and Xu, 2004; Park et al., 2003). For example, effective densities of vehicle-emitted particles with mobility diameters of 200 nm may be <0.3 g $cm^{-3}$, a factor of 5 lower than that value assumed here (Maricq and Xu, 2004). The true estimates of traffic-OA likely fall between the ACSM-HOA and SMPS-based estimation. However, these two estimates may be considered as bounding cases. Further efforts should be made to investigate the closure of estimates from different instruments and approaches.

**References**


DeCarlo, P. F., Slowik, J. G., Worsnop, D. R., Davidovits, P. and Jimenez, J. L.: Particle Morphology and Density Characterization by Combined Mobility and Aerodynamic Diameter Measurements. Part 1: Theory, Aerosol Sci. Technol., 38(12), 1185–1205, doi:10.1080/027868290903907, 2004.

Donahue, N. M., Robinson, A. L., Stanier, C. O. and Pandis, S. N.: Coupled Partitioning, Dilution, and Chemical Aging of Semivolatile Organics, Environ. Sci. Technol., 40(8), 2635–2643, doi:10.1021/es052297c, 2006.

Kuwata, M., Zorn, S. R. and Martin, S. T.: Using Elemental Ratios to Predict the Density of Organic Material Composed of Carbon, Hydrogen, and Oxygen, Environ. Sci. Technol., 46(2), 787–794, doi:10.1021/es202525q, 2012.

Maricq, M. M. and Xu, N.: The effective density and fractal dimension of soot particles from premixed flames and motor vehicle exhaust, J. Aerosol Sci., 35(10), 1251–1274, doi:10.1016/j.jaerosci.2004.05.002, 2004.

May, A. A., Presto, A. A., Hennigan, C. J., Nguyen, N. T., Gordon, T. D. and Robinson, A. L.: Gas-particle partitioning of primary organic aerosol emissions: (1) Gasoline vehicle exhaust, Atmos. Environ., 77, 128–139, doi:10.1016/j.atmosenv.2013.04.060, 2013.

Ng, N. L., Canagaratna, M. R., Jimenez, J. L., Zhang, Q., Ulbrich, I. M. and Worsnop, D. R.: Real-Time Methods for Estimating Organic Component Mass Concentrations from Aerosol Mass Spectrometer Data, Environ. Sci. Technol., 45(3), 910–916, doi:10.1021/es102951k, 2011.

Park, K., Cao, F., Kittelson, D. B. and McMurry, P. H.: Relationship between Particle Mass and Mobility for Diesel Exhaust Particles, Environ. Sci. Technol., 37(3), 577–583, doi:10.1021/es025960v, 2003.

Ranjan, M., Presto, A. A., May, A. A. and Robinson, A. L.: Temperature Dependence of Gas–Particle Partitioning of Primary Organic Aerosol Emissions from a Small Diesel Engine, Aerosol Sci. Technol., 46(1), 13–21, doi:10.1080/02786826.2011.602761, 2012.

Saha, P. K., Khlystov, A. and Grieshop, A. P.: Determining Aerosol Volatility Parameters Using a “Dual Thermodenuder” System: Application to Laboratory-Generated Organic Aerosols, Aerosol Sci. Technol., 49(8), 620–632, doi:10.1080/02786826.2015.1056769, 2015.